

ELECTRONIC SUPPLEMENTARY INFORMATION

Exploring a Hybrid Ferroelectric with 1-D Perovskite-like Structure: Bis(Pyrrolidinium) Pentachloroantimonate(III)

Martyna Ksiądzyna^a, Anna Gągor^b, Anna Piecha-Bisiorek^{a*}, Ryszard Jakubas^a,
Agnieszka Ciżman^c, Wojciech Medycki^d

(a) Faculty of Chemistry, University of Wrocław, F. Joliot-Curie 14, 50-383 Wrocław, Poland.
E-mail: anna.piecha@chem.uni.wroc.pl

(b) W. Trzebiatowski Institute of Low Temperature and Structure Research Polish Academy of Sciences, P.O. Box 1410, 50-950 Wrocław, Poland.

(c) Department of Experimental Physics, Faculty of Fundamental Problems of Technology, University of Science and Technology, Wybrzeże Wyspiańskiego 27, 50 – 370 Wrocław, Poland.

(d) Institute of Molecular Physics, Polish Academy of Sciences , M. Smoluchowskiego 17, 60-179 Poznań,
Poland.

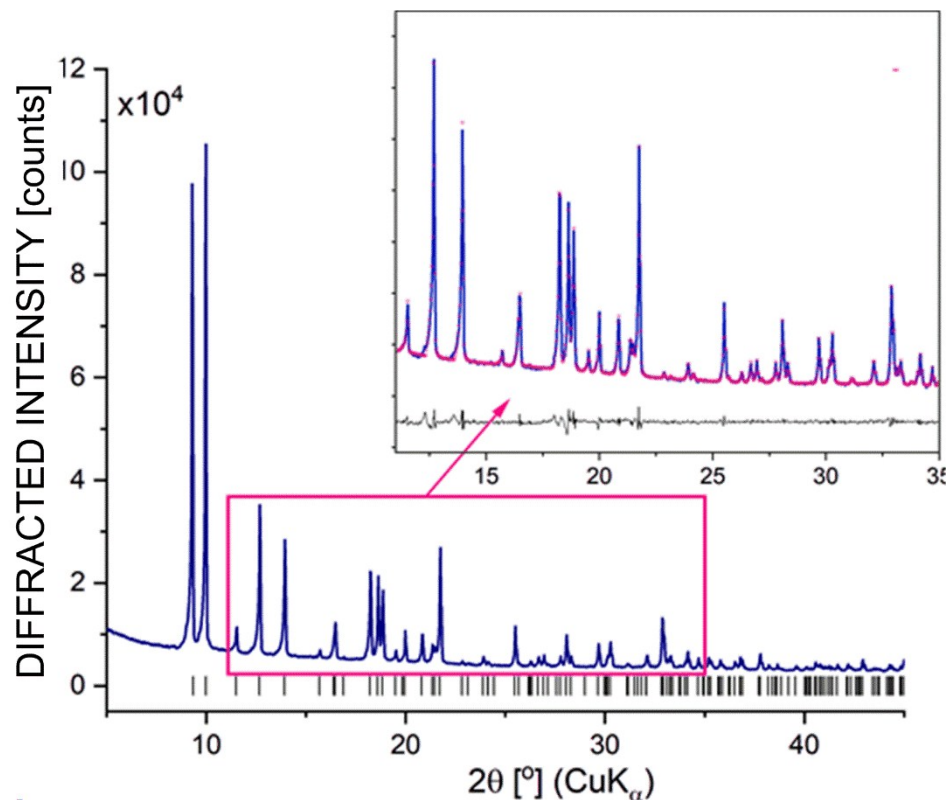


Fig. S1. Powder diffraction diagram of PCA and results of the La-Bail refinement in the inset (Jana2006). The excellent fit confirms purity of the powder samples.

Table S1. Selected geometric parameters (\AA , $^{\circ}$)

(270 K)			
Sb1—Cl1	2.408 (3)	Sb1—Cl3	2.811 (7)
Sb1—Cl1 ⁱ	2.408 (3)	Sb1—Cl4	2.9994 (6)
Sb1—Cl2	2.494 (5)	Sb1—Cl4 ⁱⁱ	2.9994 (6)
(255 K)			
Sb1—Cl10 ⁱⁱⁱ	2.402 (6)	Sb2—Cl12 ^{iv}	2.409 (5)
Sb1—Cl10	2.402 (6)	Sb2—Cl12	2.409 (5)
Sb1—Cl20	2.506 (9)	Sb2—Cl21	2.469 (7)
Sb1—Cl30	2.780 (11)	Sb2—Cl40	2.972 (6)
Sb1—Cl40	3.043 (6)	Sb2—Cl40 ^{iv}	2.972 (6)
Sb1—Cl40 ⁱⁱⁱ	3.043 (6)	Sb2—Cl31	2.921 (7)

(240 K)			
Sb1—Cl10	2.387 (8)	Sb2—Cl12	2.393 (9)
Sb1—Cl11	2.405 (8)	Sb2—Cl21	2.432 (6)
Sb1—Cl20	2.456 (8)	Sb2—Cl13	2.443 (8)
Sb1—Cl30	2.833 (8)	Sb2—Cl41	2.942 (7)
Sb1—Cl41	3.049 (7)	Sb2—Cl40	3.031 (7)
Sb1—Cl40	3.098 (7)	Sb2—Cl31	2.991 (7)
(150 K)			
Sb1—Cl10	2.4042 (16)	Sb2—Cl13	2.4306 (18)
Sb1—Cl11	2.4194 (19)	Sb2—Cl12	2.4384 (17)
Sb1—Cl20	2.4893 (19)	Sb2—Cl21	2.4406 (17)
Sb1—Cl30	2.8004 (15)	Sb2—Cl40 ^v	2.9690 (18)
Sb1—Cl40	3.0433 (18)	Sb2—Cl41	3.0244 (16)
Sb1—Cl41	3.1939 (16)	Sb2—Cl31	2.9999(17)
(270 K)			
Cl1—Sb1—Cl1 ⁱ	90.2 (2)	Cl2—Sb1—Cl4	87.00 (10)
Cl1—Sb1—Cl2	90.79 (16)	Cl3—Sb1—Cl4	92.21 (19)
Cl1 ⁱ —Sb1—Cl2	90.79 (16)	Cl1—Sb1—Cl4 ⁱⁱ	177.77 (13)
Cl1—Sb1—Cl3	90.0 (2)	Cl1 ⁱ —Sb1—Cl4 ⁱⁱ	89.49 (11)
Cl1 ⁱ —Sb1—Cl3	90.0 (2)	Cl2—Sb1—Cl4 ⁱⁱ	87.00 (10)
Cl2—Sb1—Cl3	178.9 (3)	Cl3—Sb1—Cl4 ⁱⁱ	92.21 (19)
Cl1—Sb1—Cl4	89.49 (11)	Cl4—Sb1—Cl4 ⁱⁱ	90.75 (2)
Cl1 ⁱ —Sb1—Cl4	177.77 (13)		
(255 K)			
Cl10 ⁱⁱⁱ —Sb1—Cl10	90.2 (4)	Cl12 ^{iv} —Sb2—Cl21	90.7 (2)
Cl10 ⁱⁱⁱ —Sb1—Cl20	90.5 (3)	Cl12—Sb2—Cl21	90.7 (2)
Cl10—Sb1—Cl20	90.5 (3)	Cl12 ^{iv} —Sb2—Cl40	89.0 (2)
Cl10 ⁱⁱⁱ —Sb1—Cl30	87.1 (3)	Cl12—Sb2—Cl40	176.4 (2)
Cl10—Sb1—Cl30	87.1 (3)	Cl21—Sb2—Cl40	85.7 (2)
Cl20—Sb1—Cl30	176.5 (4)	Cl12 ^{iv} —Sb2—Cl31	25.19 (17)
Cl10 ⁱⁱⁱ —Sb1—Cl40	90.0 (2)	Cl12—Sb2—Cl31	69.55 (16)
Cl10—Sb1—Cl40	178.5 (2)	Cl21—Sb2—Cl31	77.58 (19)
Cl20—Sb1—Cl40	88.0 (2)	Cl40—Sb2—Cl31	109.08 (16)
Cl30—Sb1—Cl40	94.4 (3)	Sb2—Cl40—Sb1	173.7 (3)

Cl12 ^{iv} —Sb2—Cl12	90.5 (3)		
(240 K)			
Cl10—Sb1—Cl11	91.4 (4)	Cl12—Sb2—Cl13	91.4 (4)
Cl10—Sb1—Cl20	90.9 (5)	Cl21—Sb2—Cl13	90.3 (4)
Cl11—Sb1—Cl20	89.0 (4)	Cl12—Sb2—Cl41	89.1 (3)
Cl10—Sb1—Cl30	90.3 (4)	Cl21—Sb2—Cl41	85.8 (3)
Cl11—Sb1—Cl30	84.0 (3)	Cl13—Sb2—Cl41	176.1 (3)
Cl20—Sb1—Cl30	172.9 (4)	Cl12—Sb2—Cl40	174.8 (4)
Cl10—Sb1—Cl41	176.2 (4)	Cl21—Sb2—Cl40	82.6 (3)
Cl11—Sb1—Cl41	87.9 (3)	Cl13—Sb2—Cl40	89.5 (3)
Cl20—Sb1—Cl41	92.8 (4)	Cl41—Sb2—Cl40	89.7 (2)
Cl30—Sb1—Cl41	85.9 (2)	Sb2—Cl41—Sb1	165.2 (3)
Cl12—Sb2—Cl21	92.3 (4)		
(150 K)			
Cl10—Sb1—Cl11	90.91 (6)	Cl30—Sb1—Cl41	103.70 (4)
Cl10—Sb1—Cl20	89.12 (6)	Cl40—Sb1—Cl41	88.70 (5)
Cl11—Sb1—Cl20	90.73 (9)	Cl13—Sb2—Cl12	92.14 (6)
Cl10—Sb1—Cl30	83.99 (5)	Cl13—Sb2—Cl21	91.44 (7)
Cl11—Sb1—Cl30	89.19 (6)	Cl12—Sb2—Cl21	89.35 (6)
Cl20—Sb1—Cl30	173.10 (6)	Cl13—Sb2—Cl40 ^v	89.42 (6)
Cl10—Sb1—Cl40	88.78 (5)	Cl12—Sb2—Cl40 ^v	176.19 (6)
Cl11—Sb1—Cl40	171.99 (7)	Cl21—Sb2—Cl40 ^v	87.14 (6)
Cl20—Sb1—Cl40	97.26 (7)	Cl13—Sb2—Cl41	173.02 (6)
Cl30—Sb1—Cl40	82.82 (5)	Cl12—Sb2—Cl41	88.86 (5)
Cl10—Sb1—Cl41	171.54 (5)	Cl21—Sb2—Cl41	81.66 (5)
Cl11—Sb1—Cl41	92.71 (6)	Cl40 ^v —Sb2—Cl41	89.17 (5)
Cl20—Sb1—Cl41	83.20 (6)	Sb2—Cl41—Sb1	162.73 (6)

Symmetry code(s): (i) $-x+1/2, y, z$; (ii) $x+1/2, -y+1, -z-1$; (iii) $-x, y, z$; (iv) $-x-1, y, z$; (v) $x+1, y, z$.

Table S2. Selected hydrogen-bond parameters

D—H···A	D—H (Å)	H···A (Å)	D···A (Å)	D—H···A (°)
(240 K)				
N5—H5A···Cl30	0.89	2.53	3.33 (3)	149.6
N5—H5B···Cl40	0.89	2.61	3.44 (3)	154.2
N6—H6A···Cl13	0.89	2.82	3.47 (2)	131.1
N6—H6A···Cl40	0.89	2.59	3.29 (2)	135.5
N6—H6B···Cl41 ⁱⁱ	0.89	2.33	3.21 (3)	169.5
N13—H13A···Cl31 ⁱⁱⁱ	0.89	2.37	3.20 (4)	155.7
N13—H13B···Cl20 ^{iv}	0.89	2.66	3.34 (4)	134.1
N13—H13B···Cl40 ⁱⁱ	0.89	2.73	3.35 (3)	127.9
N17—H17A···Cl30 ^v	0.89	2.37	3.24 (3)	163.9
N17—H17B···Cl31 ⁱⁱⁱ	0.89	2.27	3.14 (3)	164.0
(150 K)				
N5—H5A···Cl31 ^{vi}	0.89	2.24	3.114 (5)	167.0
N5—H5B···Cl20 ^{vi}	0.89	2.55	3.315 (6)	144.8
N5—H5B···Cl41 ^{vi}	0.89	2.72	3.280 (5)	121.9
N8—H8A···Cl30 ^{vii}	0.89	2.34	3.202 (6)	162.5
N8—H8B···Cl31 ^{vi}	0.89	2.28	3.137 (5)	160.8
N15—H15A···Cl30 ^{viii}	0.89	2.46	3.237 (5)	146.7
N15—H15B···Cl41 ^{vii}	0.89	2.45	3.276 (5)	155.0
N16—H16A···Cl40	0.89	2.30	3.187 (6)	177.6
N16—H16B···Cl12	0.89	2.80	3.447 (5)	130.6
N16—H16B···Cl41	0.89	2.59	3.248 (5)	131.4

Symmetry code(s): (i) $x+1/2, -y+1, -z-1$; (ii) $x+1, y, z$; (iii) $x+1/2, -y, z-1/2$; (iv) $x+3/2, -y, z-1/2$; (v) $x+1/2, -y+1, z-1/2$; (vi) $x-1, y, z$; (vii) $x, y-1, z$; (viii) $x+1, y-1, z$.

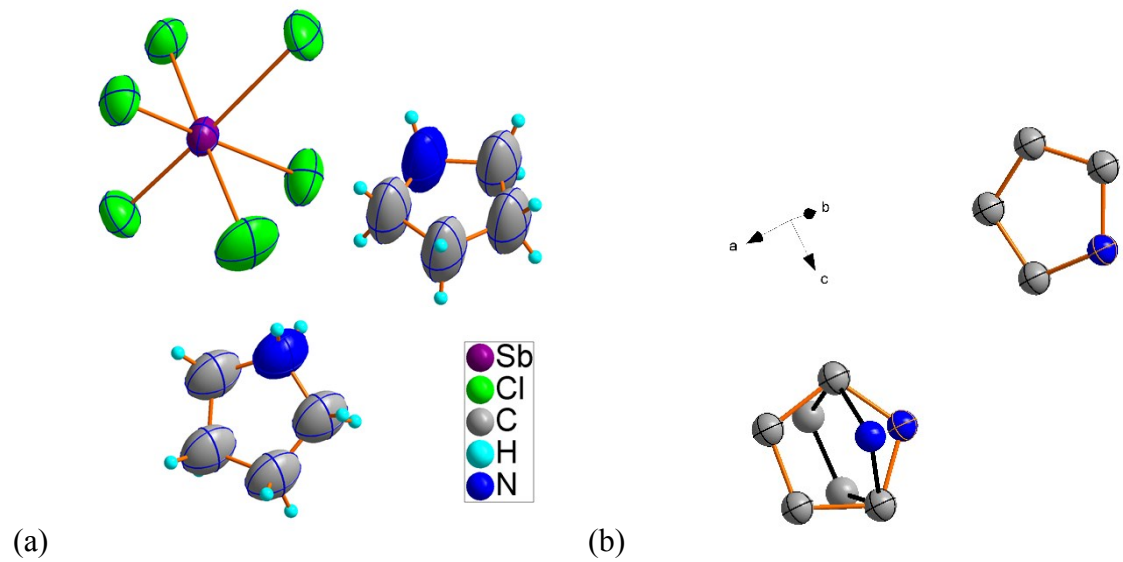


Fig. S2 (a) The content of the asymmetric unit in Phase I, $T=270$ K;
 (b) the disorder of Pyr^+ in Phase I.

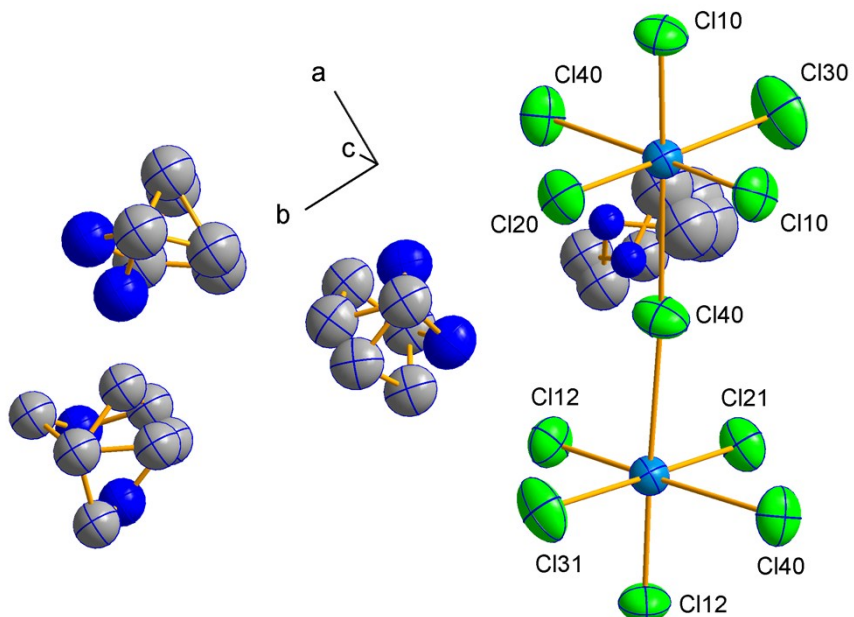


Fig. S3. The content of the asymmetric unit in Phase II, $T=255$ K, the ellipsoids are drawn at 25% probability level.

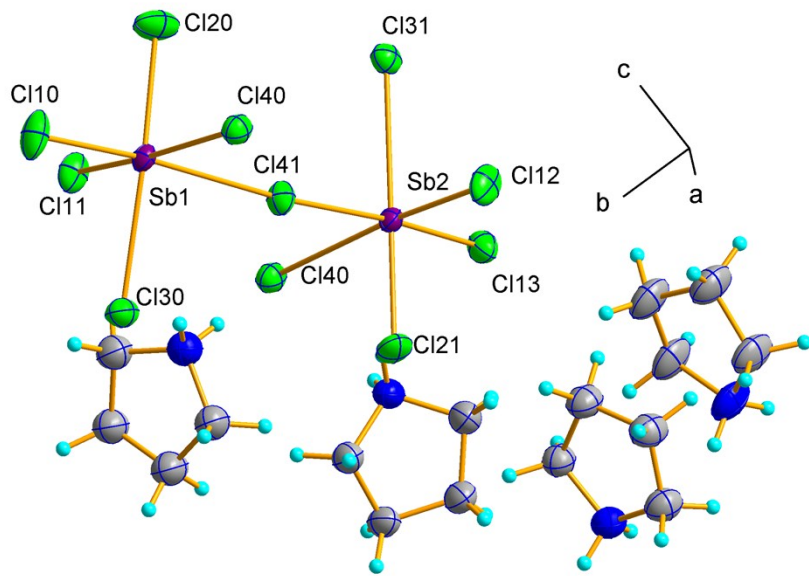


Fig. S4. the content of the asymmetric unit in Phase III, $T=240\text{ K}$, the ellipsoids are drawn at 25% probability level.

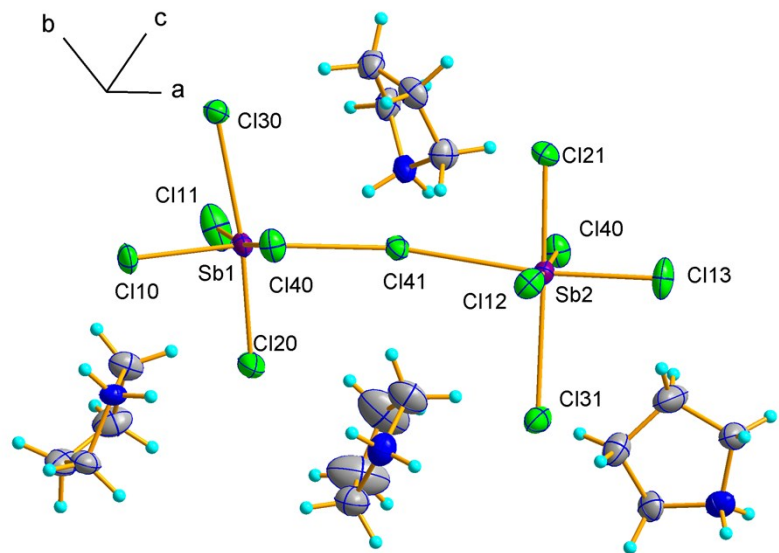


Fig. S5. The content of the asymmetric unit in Phase IV, $T=150\text{ K}$, the ellipsoids are drawn at 50% probability level.

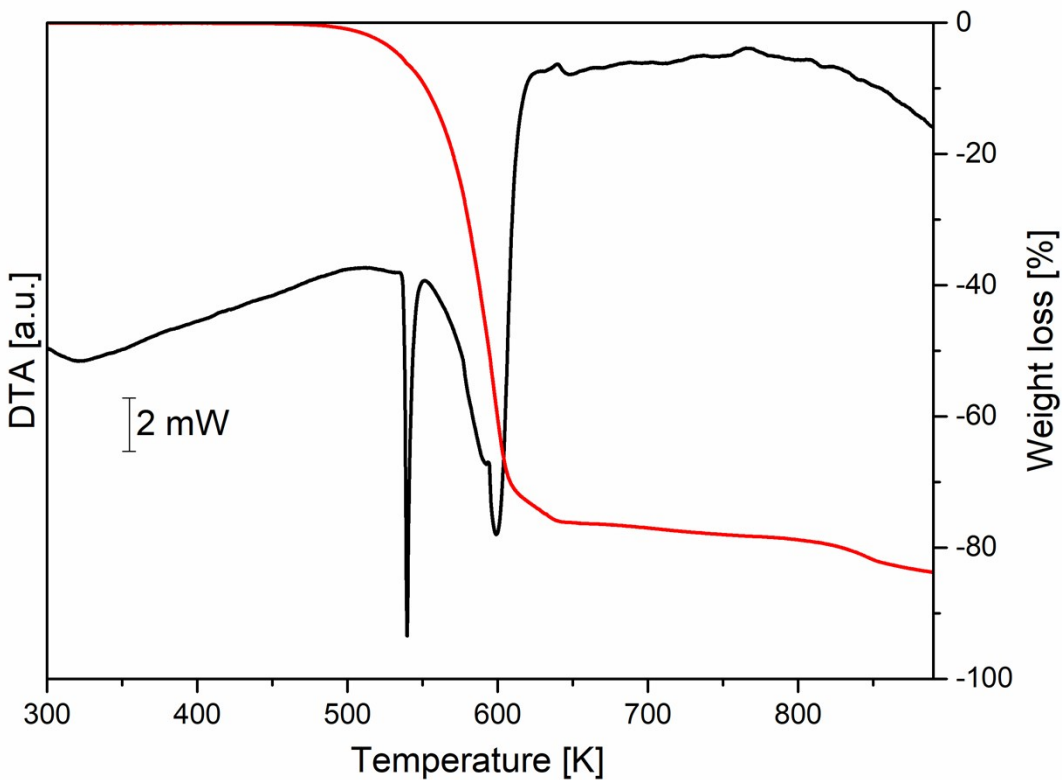


Fig. S6. Thermograms of TGA and DTA.

Table S3. The results of the symmetry mode analysis, phase transition I to II (distortion of the inorganic part of the structure).

WP		Atom	Atomic Displacements			
			ux	uy	uz	u
2a	(0,y,z)	Sb1	0.0000	-0.0172	-0.0015	0.1931
2a	(0,y,z)	Sb1_2	0.0000	-0.0180	-0.0014	0.2010
4b	(x,y,z)	Cl4	0.0019	-0.0224	-0.0100	0.3064
2a	(0,y,z)	Cl2	0.0000	-0.0066	-0.0043	0.1059
2a	(0,y,z)	Cl2_2	0.0000	-0.0084	-0.0048	0.1265
2a	(0,y,z)	Cl3	0.0000	-0.0227	0.0085	0.2944
2a	(0,y,z)	Cl3_2	0.0000	-0.0401	0.0135	0.5063
4b	(x,y,z)	Cl1	-0.0009	-0.0127	0.0020	0.1456
4b	(x,y,z)	Cl1_2	0.0018	-0.0105	0.0029	0.1286

NOTE: ux, uy and uz are given in relative units. |u| is the absolute distance given in Å; Maximum atomic displacement in the distortion, Δ: 0.5063 Å. Total distortion amplitude: 1.1926 Å (Pnma 0.2182 Å, Pmn2_1 1.1724 Å).

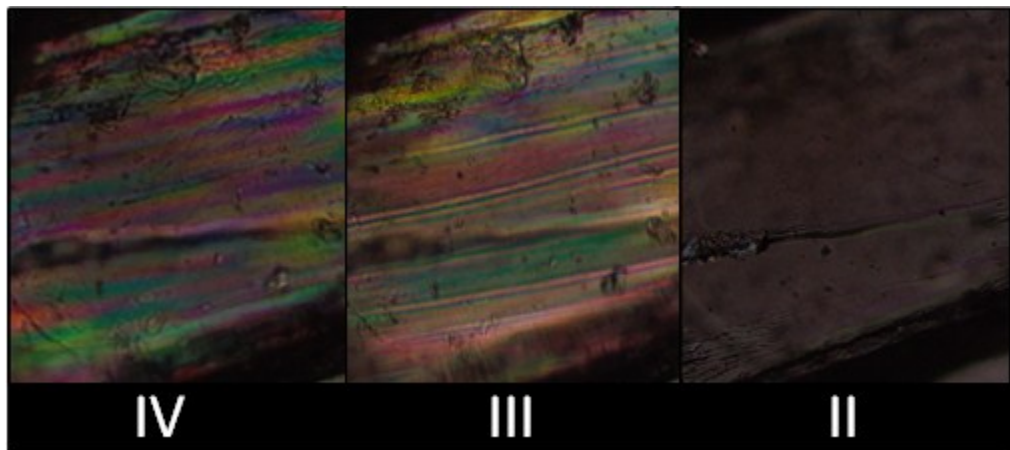


Fig. S7. Evolution of the domain structures at different phases.

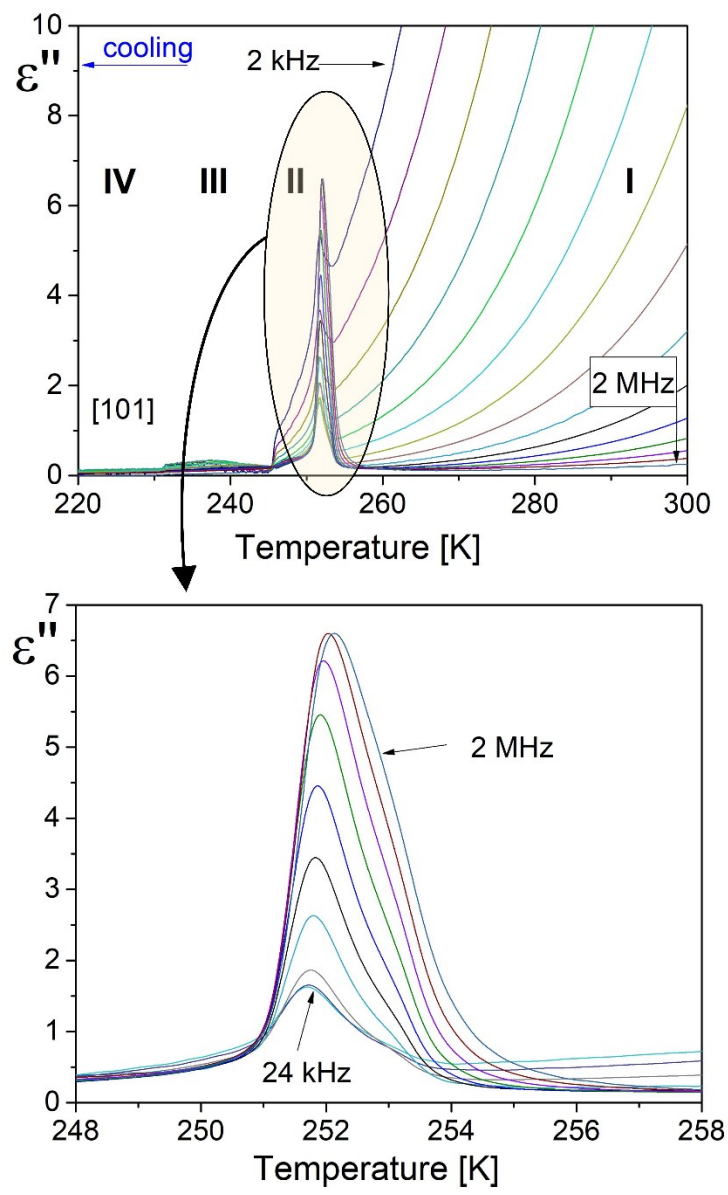


Fig. S8. Imaginary part of complex electric permittivity measured along the [101] direction during cooling.

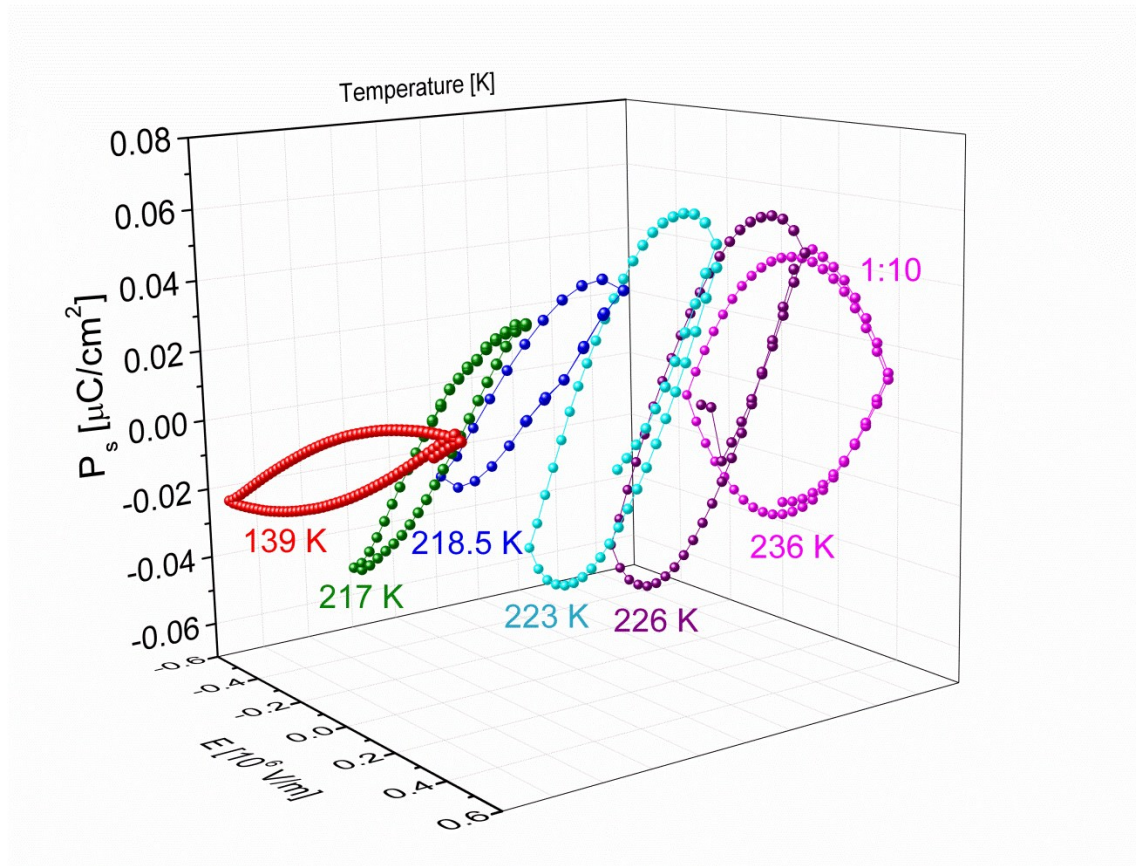


Fig. S9. Evolution of hysteresis loops between 139 K and 236 K.

Table S4. Activation energies, correlation times and motional constants evaluated for PCA.

Temperature range	Component	E _a (kJ/mol)	τ ₀ [s]	C [s ⁻²]
- 120 K		5.56	1.6 10 ⁻¹²	4.35 10 ⁸
120 K-170 K	short	7.81	5.7 10 ⁻¹²	3.82 10 ⁸
197 K-244 K		22.82	2.85 10 ⁻¹⁴	1.38 10 ⁸
248 K -		12.2		

The temperature dependence of the second moment of the proton resonance lines (M_2) of PCA is shown in Fig. S10. It is seen that between 95 and 140 K the second moment has a plateau of about 19 G². Above 140 K the two reduction of the M_2 are visible. First reduction $\Delta M_2(1)$ occurs around 170 and the next one $\Delta M_2(2)$ around 240 K. The continually decreasing

of the M_2 values is abruptly broken close to PTs temperature at 248 and at 255 K. The remaining PT at 236 K is not reflected in the observed course of M_2 reductions. Through the PTs at 248 K and 255 K a sharp decrease in the second moment from 7.3 G² to 4.1 G² is visible. After next narrowing of the proton NMR line the values of the M_2 stabilize at about 3.2 G² up to 290 K which means that the full isotropic motion of the pyrrolidinium cation is still not reached.

The basic equation for the dipolar second moment, M_2 , of a dipolar NMR line was derived by equation:¹

$$M_2 = \frac{3}{5} I(I+1) \gamma^2 \hbar^2 \frac{1}{N} \sum_{i=1}^N \sum_{j=1}^N R_{ij}^{-6} \quad (1)$$

where N is the number of protons in the unit cell. The rigid value of M_2 calculated from the crystal structure of PCA appeared to be about 20.1 G² with assumed lengths of bonds: C-H 1.09 Å and N-H 1.03 Å. Such result of theoretical calculation shows almost perfect compatibility with measured experimental value and it should be emphasized the lack of any disturbing quadrupole interaction of neighboring quadrupole nuclei.^{2,3} Analysis of the temperature dependence of M_2 can be performed on the basis of the BPP formula:

$$M_2 = \Delta M_2(1) \frac{2}{\pi} \tan^{-1}(\gamma_H \tau_c \sqrt{M_2}) + \Delta M_2(2) \frac{2}{\pi} \tan^{-1}(\gamma_H \tau_c \sqrt{M_2}) + M_2^{\text{Motion}} \quad (2)$$

where $\tau_c = \tau_0 \exp(E_a/RT)$, M_2^{Rigid} (where $M_2^{\text{Rigid}} = \Delta M_2(1) + \Delta M_2(2) + M_2^{\text{Motion}}$) and M_2^{Motion} are the second-moment values before and after of both second moment reduction, respectively. The reduction of the second moment has been fitted with equation (2) with the activation energy of 39.47 kJ·mol⁻¹ and the correlation time of 2.98 10⁻¹⁴ s for the first reduction of M_2 and with the activation energy of 28.34 kJ·mol⁻¹ and the correlation time of 3.94 10⁻¹⁴ s for the second reduction of M_2 . Such obtained dynamical parameters are typical for planar cations.⁴

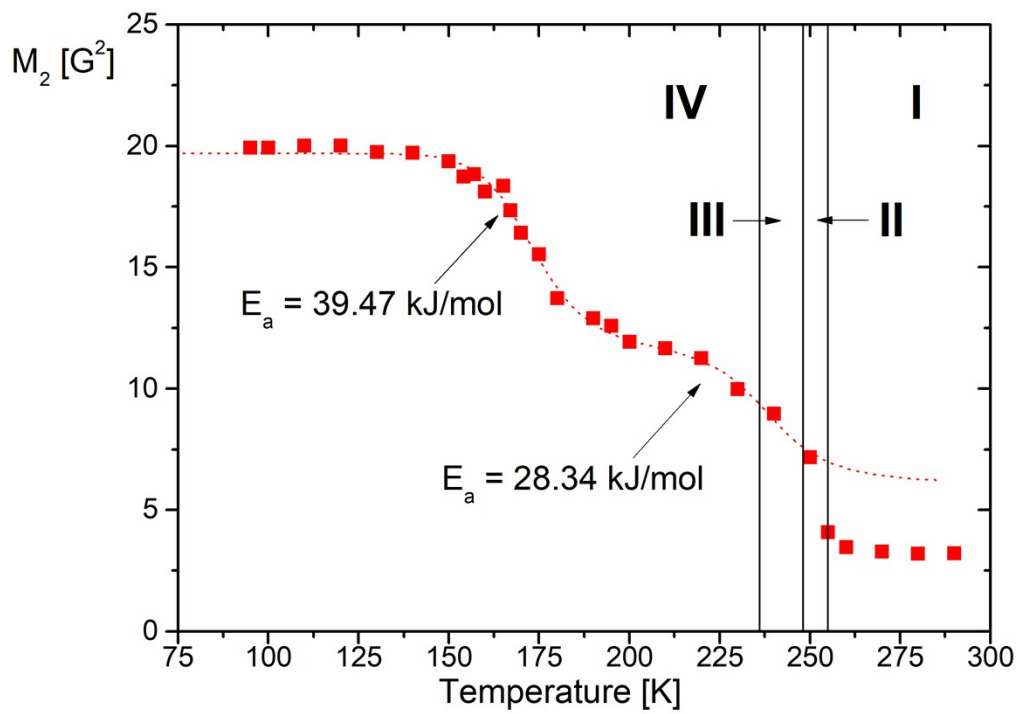


Fig. S10. Temperature dependence of the second moment (M_2) of the proton NMR lines.

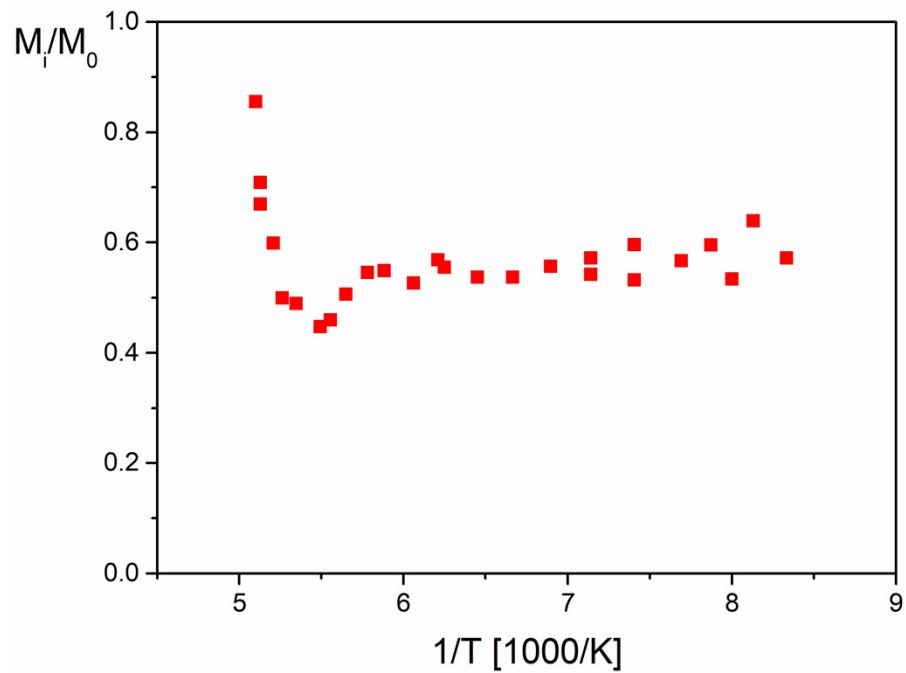


Fig. S11. Temperature dependence of the contribution of both proton magnetization for PCA.

Below 120 K and above 197 K the recovery function have one-exponential shape due to a fast spin diffusion and the only one relaxation time T_I was well-fitted from it. In turn, there is no a fast spin diffusion between 120 K and 197 K and a recovery curve should be separated into at least two relaxation times, T_I^S and T_I^L ($T_I^S < T_I^L$), according to the equation

$$(M_0 - M_z(\tau))/M_0 = A^S \exp(-\tau/T_I^S) + A^L \exp(-\tau/T_I^L) \quad (3)$$

where M_0 and $M_z(t)$ are components of magnetization at thermal equilibrium and at time τ after the saturation sequence, respectively. A^S and A^L are constants and $A^S + A^L = 1$. In the temperature range from 120 K to 197 K, the mutual relation between the two observed components seems to be in the 1:1 proportion (The temperature course of percentage proportion of one magnetization of both ones is presented in Figure S11).

- 1 J. H. Van Vleck, *Phys. Rev.*, 1948, **74**, 1168–1183.
- 2 A. Piecha, R. Jakubas, A. Pietraszko, J. Baran, W. Medycki and D. Kruk, *J. Solid State Chem.*, 2009, **182**, 2949–2960.
- 3 D. Kruk, W. Medycki, A. Mielczarek, R. Jakubas and C. Uniszkieicz, *Appl. Magn. Reson.*, 2010, **39**, 233–249.
- 4 P. Szklarz, J. Zaleski, R. Jakubas, G. Bator, W. Medycki and K. Falińska, *J. Phys. Condens. Matter*, 2005, **17**, 2509–2528.